Ordered Fe(II)Ti(IV)O_3 Mixed Monolayer Oxide on Rutile TiO_2(011)

Sandamali Halpegamage,[†] Pan Ding,[‡] Xue-Qing Gong,[‡] and Matthias Batzill*[,†]

[†]Department of Physics, University of South Florida, Tampa, Florida 33620, United States and [‡]Key Laboratory for Advanced Materials, Centre for Computational Chemistry and Research Institute of Industrial Catalysis, East China University of Science and Technology, Shanghai 200237, P.R. China

ABSTRACT Oxide monolayers supported or intermixed with an oxide support are potential nanocatalysts whose properties are determined by the interplay with the support. For fundamental studies of monolayer oxides on metal oxide supports, well-defined systems are needed, but so far, the synthesis of monolayer oxides with long-range order on single-crystal oxide surfaces is rare. Here, we show by a combination of scanning tunneling microscopy, photoemission spectroscopy, and density functional theory (DFT)-based computational analysis that the rutile TiO_2(011) surface supports the formation of an ordered mixed $FeTiO_3$ monolayer. Deposition of iron in a slightly oxidizing atmosphere (10^{-8} Torr O_2) and annealing to 300 °C results in a well-ordered surface structure with Fe in a 2+ charge state and Ti in a 4+ charge states. Low-energy ion scattering suggests that the cation surface composition is close to half Fe and half Ti. This surface is stable in ultrahigh vacuum to annealing temperatures of 300 °C before the iron is reduced. DFT simulations confirm that a surface structure with coverage of 50% FeO units is stable and forms an ordered structure. Although distinct from known bulk phases of the iron–titanium oxide systems, the $FeTiO_3$ monolayer exhibits some resemblance to the ilmenite structure, which may suggest that a variety of different mixed oxide phases (of systems that exist in a bulk ilmenite phase) may be synthesized in this way on the rutile TiO_2(011) substrate.

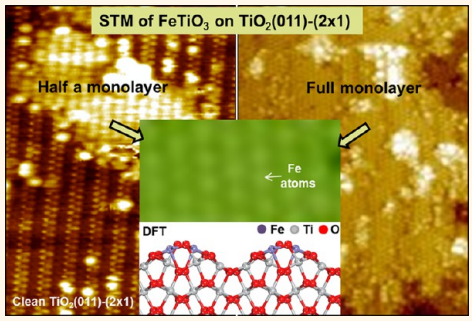

KEYWORDS: TiO_2 · FeO · mixed oxide · surface structure · nanocatalyst · scanning tunneling microscopy · single-crystal oxide surfaces

Due to their chemical stability, metal oxides have wide applications in chemical sensors, heterogeneous catalysis, and photocatalysis, *etc.* These applications are sensitive to the surface structure and composition. At the same time, the (photo)catalytic properties of transition metal oxides are being modified by bulk or surface doping with various other transition metals, creating complex systems whose fundamental structure and properties are often poorly understood. Only in a few cases are clear synergies between surface dopants and substrate oxides known. For example, a noteworthy system is vanadium oxide on a TiO_2 heterogeneous catalyst for partial oxidation reactions of alcohols to aldehydes and oxidative dehydrogenation of alkanes to alkenes. However, even in this case, details of the active vanadium oxide surface species are still debated, and a number of surface science studies of vanadia on TiO_2 have been performed in order to address possible configurations.[1] A complicating factor is that in many of these catalytically active systems different surface orientations of the oxide support can result in very different dopant species and thus chemical properties. Sometimes minority facets can dominate the activity of a catalyst, and thus the surface orientation of the support may be crucial for stabilizing catalytically active species. For instance, it is believed that for catalytic combustion of methane over Pd/CeO_2 catalysts, the formation of a mixed PdCeOx surface layer on the CeO_2(110) surface under reaction conditions could be the catalytically active phase.[2] The (110) surface exhibits formation energy much higher than that of the (111) surface[3] and thus is just a minority facet on a CeO_2 crystal. The fact that the mixed $PdCeO_2$ oxide forms on a high surface energy orientation may not be a coincidence. Surfaces with high energies are by definition less stable, often resulting in complex surface reconstructions, and thus may more readily incorporate "impurity" atoms in its crystal structure. Thus, we propose that, in an attempt to search for novel mixed oxide surface phases, one should consider surface orientations that exhibit surface

* Address correspondence to mbatzill@cas.usf.edu.

Received for review July 6, 2015 and accepted July 30, 2015.

Published online July 30, 2015
10.1021/acsnano.5b04125

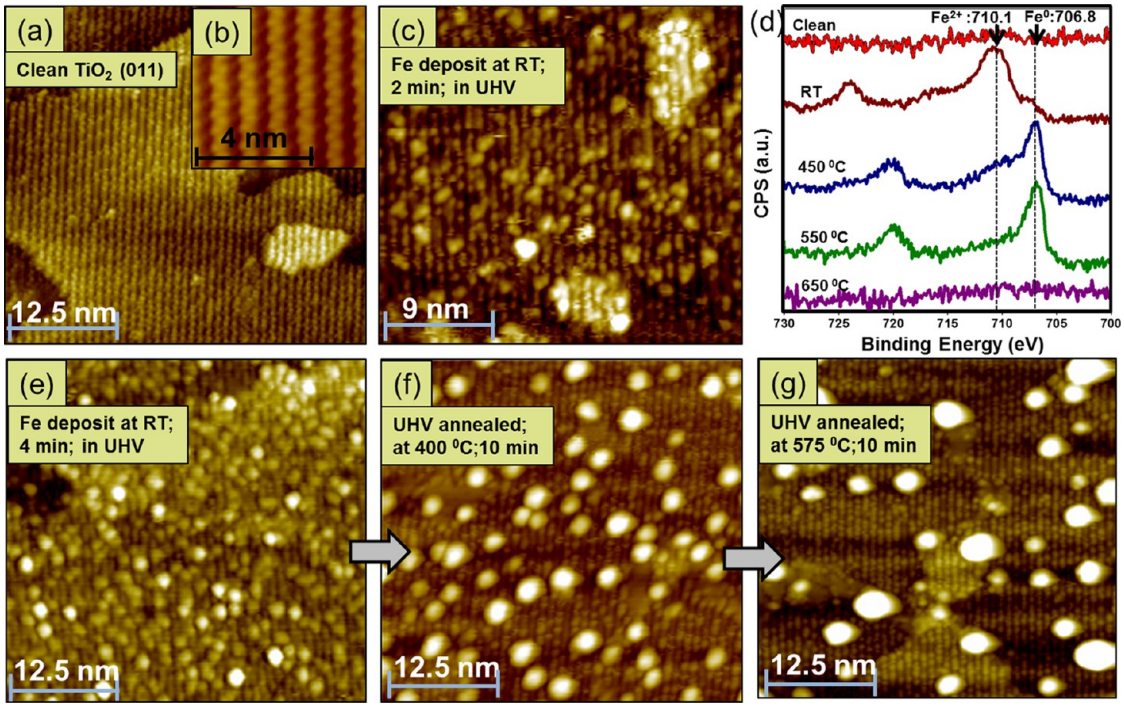

Figure 1. STM images of (a,b) the clean TiO_2(011) surface; (c,e) after depositing Fe at room temperature in UHV for 2 and 4 min; (f) after annealing 4 min Fe deposit in UHV at ~400 °C for 10 min, and (g) at 575 °C for 10 min. (d) XPS spectra for 2 min Fe deposit in UHV at room temperature and subsequent annealing for 10 min at 450, 550, and 650 °C in UHV. All STM images were taken with ~1.2 V and ~400 pA tunneling conditions.

reconstructions in their pure form. For the initial choice of the "impurity" atoms, we consider atoms that are known to form bulk mixed oxides with the support material, that is, elements that are miscible with the support material, although this may not be a necessary condition since the miscibility of oxides may be different at the surface than in the bulk.

Titanium dioxide is a model system for oxide surface science studies[4] and a prototypical photocatalyst.[5] Most surface science studies have been performed on the rutile (110) surface, which has the lowest surface formation energy and exhibits a bulk truncation with small surface relaxations. On the other hand, the second most stable surface orientation, the (011) surface, exhibits a complex surface reconstruction with a (2 × 1) periodicity[6−8] and thus may be a better candidate for stabilizing novel mixed oxide phases (see Figure 1a,b). As a potential dopant cation, we chose iron. Iron oxide and titanium oxide form various stable bulk mixed oxides. Ilmenite with an $Fe(II)Ti(IV)O_3$ composition is the most prominent mineral and common source for titanium in the Earth's crust. On the other hand, it is known for small iron impurities in rutile and anatase TiO_2 to segregate to the surface by vacuum annealing,[9,10] but no ordered mixed oxide layer at the surface has been reported previously. Here, we show that an ordered mixed oxide surface layer can form on the rutile (011) surface, which has an $Fe(II)Ti(IV)O_3$ composition and bares some structural similarities to the ilmenite phase. This oxide may form under very low oxygen partial pressure (10^{-8} Torr O_2). However, annealing in ultrahigh vacuum (UHV) results in the reduction of Fe and formation of metallic iron clusters at the surface.

RESULTS AND DISCUSSION

The preparation of an ordered mixed Fe−Ti oxide surface on TiO_2(011) is sensitive to the preparation conditions in a UHV chamber. Therefore, the experimental part focuses on the morphology, Fe oxidation state, and structural characterization as a function of preparation conditions and the thermal stability of the iron deposits. The computational part uses first-principles density functional theory (DFT) simulations combined with an evolutionary algorithm to determine the stable structures of the ordered mixed oxide phase.

Experimental. The surface structure and thermal evolution for three differently prepared iron deposits on TiO_2(011) are presented: (i) deposition of iron in UHV, (ii) iron deposition in an oxygen atmosphere of 5×10^{-8} Torr and its thermal evolution by annealing in UHV, and (iii) an optimized procedure for obtaining only the mixed oxide phase, consisting of a combination of Fe deposition in 5×10^{-8} Torr and annealing in oxygen and UHV. Iron deposition in 10^{-6} Torr O_2 was also attempted and qualitatively resulted in the same ordered structures. However, in addition to the ordered structure, clusters were formed which may be a consequence of reoxidation of bulk Ti interstitials. Thus, in the experiments, we concentrated on the

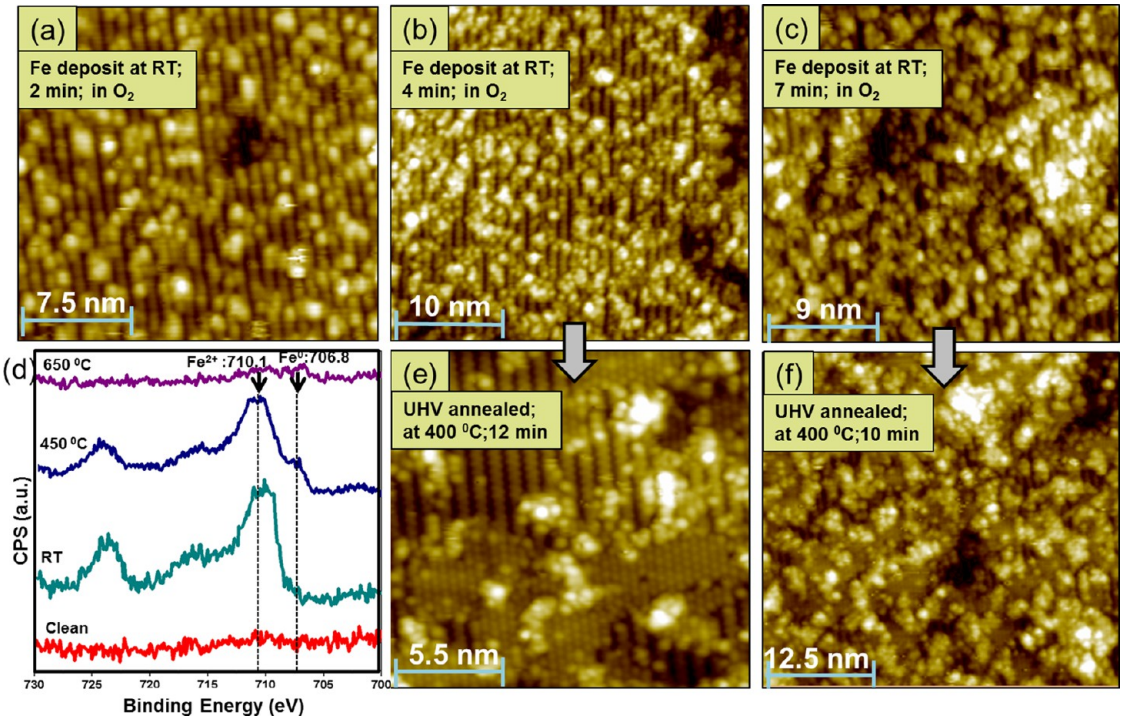

Figure 2. STM images of Fe deposited on TiO_2(011) in 5×10^{-8} Torr O_2 background pressure at room temperature for (a) 2 min, (b) 4 min, and (c) 7 min exposure periods; (e) after annealing 4 min Fe deposit in UHV at ~400 °C for 12 min; (f) after annealing 7 min Fe deposit in UHV at ~400 °C for 10 min. (d) XPS spectra for 2 min Fe deposit in 5×10^{-8} Torr O_2 background at room temperature and subsequent annealing for 10 min at 450 and 650 °C in UHV. All STM images were taken with ~1.2 V and ~400 pA tunneling conditions.

lower (5×10^{-8} Torr) pressures, and these are the results discussed here. In the following, the results for sample preparation conditions (i−iii) are discussed separately.

Fe Deposition at Room Temperature and Annealing in UHV. Fe was deposited in UHV at room temperature. Scanning tunneling microscopy (STM) images, shown in Figure 1, reveal the formation of clusters. The cluster size and density increased with deposition time. For low amounts of deposited Fe, the clusters appear flat, that is, no more than a single atomic layer in height and lateral dimensions of only 1−2 surface unit cells (see Figure 1c). With increased Fe deposition, a few thicker and bigger clusters occurred. These clusters are 2−3 atoms in height but still only a couple of surface unit cells wide (Figure 1e). Annealing of this Fe deposit in UHV led to a sintering of the iron clusters. Figure 1f,g shows samples annealed at 400 and 575 °C, respectively. To investigate the oxidation state of the deposited iron, we conducted X-ray photoemission spectroscopy (XPS) studies. After deposition of Fe at room temperature, as shown in Figure 1d, the Fe 2p peak exhibits an oxidized Fe^{2+} state with a binding energy of 710.1 eV and a metallic state with a binding energy at 706.8 eV. In addition, a satellite peak at an apparent binding energy of 715.2 eV is observed, which is a characteristic feature of FeO, corroborating the assignment of iron in a 2+ charge state. Oxidation of iron without the presence of oxygen in the atmosphere suggests a simultaneous reduction of the Ti at the interface. Indeed, a small Ti^{3+} is observed in the Ti 2p spectra in XPS. Annealing in UHV to sequentially higher temperatures causes a decrease of the Fe^{2+} component, as shown in Figure 1d. This indicates that the larger clusters observed in STM are predominantly metallic Fe. The observed decrease in the Fe^{2+} component during annealing may be a consequence of reduction of the iron at elevated temperature or diffusion of oxidized iron into the bulk. Further annealing to 650 °C results in a complete loss of iron signal in XPS and thus suggests that iron diffusing into the bulk occurs at these temperatures. Overall, the picture described here for Fe deposition without oxygen is very similar to the studies performed on TiO_2(110).[11,12]

Fe Deposition in an O_2 (5×10^{-8} Torr) Atmosphere at Room Temperature and Annealing in UHV. When Fe is deposited in a low O_2 background pressure of 5×10^{-8} Torr at room temperature, formation of metallic clusters is avoided. Figure 2a−c shows STM images for increasing deposition times in the submonolayer regime. The surface exhibits disordered structures but no large clusters. Subsequent annealing of these deposits to 400 °C in UHV also did not cause formation of larger clusters, in contrast to the UHV-deposited iron discussed above. Instead, an ordered structure was observed after annealing to 400 °C. This is shown in Figure 2e,f. This structure is less corrugated than the 2×1 reconstruction of the pure TiO_2(011) surface but

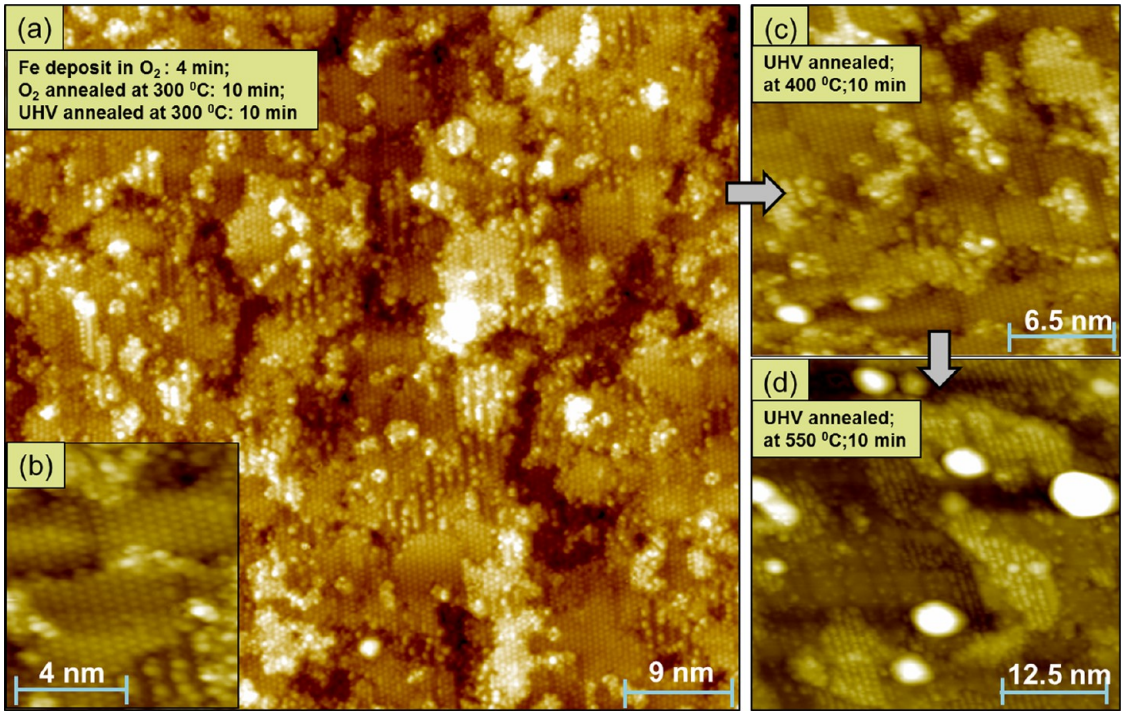

Figure 3. STM images of (a) Fe deposited on TiO_2(011) in 5 × 10^{-8} Torr O_2 background pressure at room temperature for 4 min exposure period and annealed immediately in 5 × 10^{-8} Torr O_2 at ~300 °C for 10 min followed by UHV annealing for about 10 min. (b) High-resolution STM of Fe−Ti mixed oxide phase. (c) After annealing, the new structure in UHV ~ 400 °C for 10 min and (d) after annealing in UHV at ~550 °C for 10 min. All STM images were taken with ~1.2 V and ~400 pA tunneling conditions.

may still be described as a 2 × 1 superstructure with respect to the (011) substrate. The structural details are discussed below. However, in addition to the two ordered surface structures (*i.e.*, the clean TiO_2(011)-2 × 1 and the new ordered mixed FeTi oxide), there still remain many small clusters at the surface. In XPS, only Fe^{2+} is observed for the as-deposited Fe (in oxygen atmosphere) as well as for samples annealed to temperatures as high as 300 °C in UHV. At higher annealing temperatures, metallic iron was eventually formed, as indicated in the XPS spectra shown in Figure 2d. Higher annealing temperatures are discussed below for samples that start off with a more uniform mixed oxide surface, the preparation of which is discussed next.

Optimized Preparation for Ordered Mixed Fe−Ti Surface Phase. In an attempt to prepare surfaces that are predominantly covered with the mixed Fe−Ti oxide surface, we combined Fe deposition and annealing in an oxygen atmosphere with vacuum annealing at 300 °C, that is, a temperature for which we have demonstrated that the new phase is stable in UHV without reduction of the iron. We found that the best preparation conditions consist of room temperature deposition of Fe in 5 × 10^{-8} Torr O_2, immediately followed by annealing of the sample at 300 °C in the same oxygen background for 10 min. Then the O_2 was turned off, and the sample was annealed for another 5−10 min at the same temperature in UHV. Such prepared samples exhibit up to 90% of the surface covered with the new mixed Fe−Ti oxide phase, as the STM image in Figure 3a shows. To obtain information about the composition of this surface layer, we conducted low-energy ion scattering spectroscopy (ISS) experiments using He^+ ions. Due to the high probability of He neutralization, this technique is very surface sensitive and primarily probes the surface composition of the topmost layer. Figure 4 shows the ISS data for the pristine TiO_2 surface and the surface ~90% covered with the new surface phase. For the latter, the Fe peak is only slightly more intense than the Ti peak. Given the unknown neutralization cross sections for He^+ scattered from Ti and Fe, it is impossible to quantitatively determine the composition of the surface layer. However, the similar intensities for Ti and Fe suggest a close to 1:1 composition in the surface layer.

Further vacuum annealing of the same mixed surface oxide sample at 400 °C for 10 min in UHV results in the formation of small clusters, as shown in the STM image in Figure 3c. With higher annealing temperatures, the size of these clusters increases, which can be seen from Figure 3d for an annealing temperature of 550 °C. A systematic XPS study of the oxidation state of Fe as a function of annealing temperature is shown in Figure 5. At 300 °C, no metallic iron is detected, and with increasing annealing temperature, the ratio of metallic Fe to Fe^{2+} continues to increase. The change of the Fe^{2+} and metallic Fe peak intensity as a function of annealing temperature and normalized to the Ti 2p

intensity shows the rapid decrease in intensity of the Fe^{2+} signal while the metallic component increases only weakly; in other words, the total Fe signal decreases with annealing temperatures. This difference in the apparent rate of change of the two components is likely a consequence of the different morphologies. The metallic iron is assumed to be mainly present in the clusters that are seen in STM occurring on the surface after annealing, while the Fe^{2+} signal comes, at least initially, from the 2D surface oxide phase. The higher sensitivity of XPS to dispersed species at the surface compared to iron in clusters can explain the overall (metallic plus Fe^{2+}) decrease in the Fe 2p signal with annealing temperature. Furthermore, some loss of Fe^{2+} species through diffusion into the bulk is likely. We also monitored the Ti 2p and O 1s signals. For the Ti signal, we did not observe any additional formation of Ti^{3+} or lower oxidation states. Thus, the formation of the mixed oxide surface appears to only consist of Ti^{4+} and Fe^{2+}. A rigid shift of ~0.2 eV of the entire Ti 2p peak and the O 1s peak was observed upon formation of the Fe−Ti mixed surface oxide compared to the pristine TiO_2(011)-2 × 1 surface. Such a shift is caused by an upward band bending of the TiO_2 at the surface, implying the formation of a positive space charge region in TiO_2 induced by the mixed oxide surface layer. In addition to core level photoemission spectroscopy, we utilized ultraviolet photoemission spectroscopy (UPS) to monitor the formation of new valence band states. Figure 6 shows the valence bands of the pristine TiO_2(011)-2 × 1 surface and the valence band after formation of the mixed $FeTiO_x$ surface oxide. The valence band maximum for the pristine TiO_2(011) surface is determined to be ~2.8 eV below the Fermi level, consistent with a strongly n-type doped rutile TiO_2 sample. Some photoemission intensity was observed within the band gap. This is a combination from photoemission excited by the non-monochromatic He lamp as well as defect-induced true band gap states in

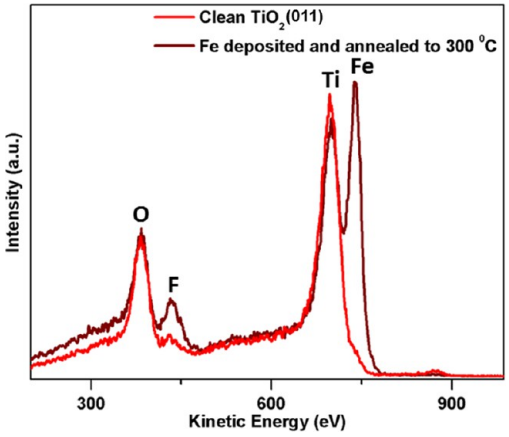

Figure 4. Ion scattering spectra for the TiO_2(011) surface before and after deposition of Fe at room temperature in 5×10^{-8} Torr of O_2 and annealing at ~300 °C in the same oxygen background (the fluorine peak is a contamination).

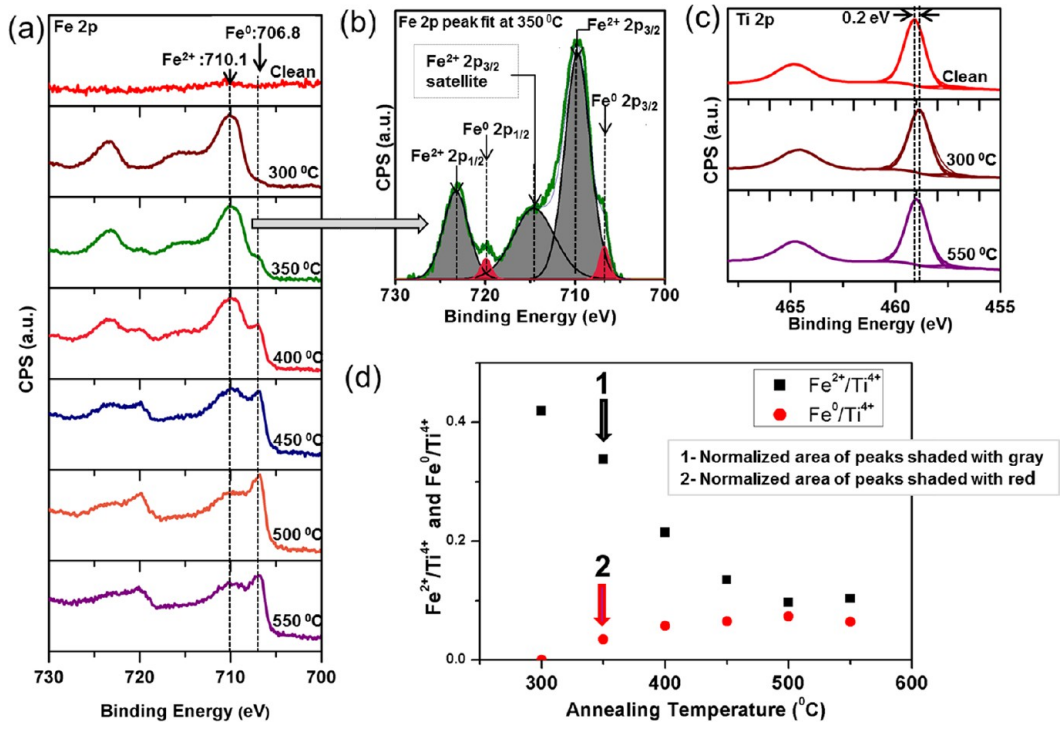

Figure 5. X-ray photoemission studies of Fe deposition on TiO_2(011) for (a) room temperature Fe deposition and annealing to 550 °C from 300 °C in steps of 50 °C in O_2 background pressure of 5×10^{-8} Torr. (b) Peak fitting for 350 °C annealed Fe deposit (the same fitting parameters were maintained for all other Fe 2p spectra in (a)). (c) Ti 2p peak for clean TiO_2(011) surface and for the Fe-deposited and annealed samples at 350 and 550 °C. (d) Fe^{2+}/Ti^{4+} and Fe^0/Ti^{4+} ratios with the annealing temperature.

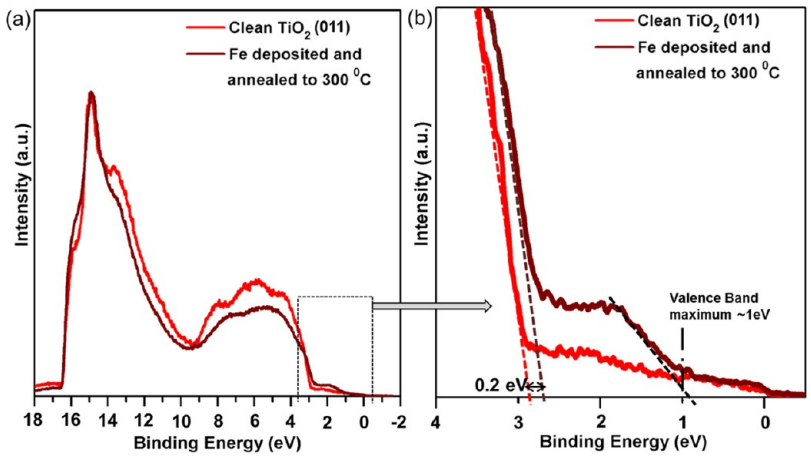

Figure 6. (a) UV photoemission spectroscopy for the TiO_2(011)-(2 × 1) sample before and after Fe deposition at room temperature in 5 × 10^{-8} Torr of O_2 and annealing to 300 °C in the same oxygen background; (b) zoomed-in view of the low BE region.

TiO_2.[13−15] Upon formation of the mixed $FeTiO_x$ surface oxide, a significant band gap narrowing was observed. The new valence band maximum is measured around 1.0 eV below the Fermi level, and we attribute this new valence band maximum within the bulk band gap of TiO_2 to the valence band of the mixed surface oxide. This valence band maximum may be compared to known bulk band gaps for ilmenite $Fe^{2+}Ti^{4+}O_3$ of 2.5−2.9.[16−18] This means that either the surface mixed oxide has a much reduced band gap or the Fermi level lies closer to midgap than it does for the TiO_2 substrate.

Scanning Tunneling Microscopy of Ordered Structure. The experimental studies suggest the formation of a mixed surface oxide with Fe/Ti ratio of about 1:1 and Fe in the 2+ oxidation state. STM shows a well-ordered structure with the same periodicity as the reconstructed pristine TiO_2(011)-2 × 1 surface, that is, a rectangular unit cell. Two protrusions per unit cell are imaged, that is, a protrusion in every corner of the rectangular unit cell and another protrusion close to the center of the unit cell, as schematically illustrated in Figure 7a. From STM, this gives a surface structure that may be described as a c(2 × 1) unit cell. Previously, we reported a similar structure after oxygen annealing of the pristine TiO_2(011) surface.[19] Because of the similarities in the STM images as well as the valence band, it is possible that the previously reported structure, in fact, was formed by iron impurity segregation and not a separate TiO_2 surface phase. The STM image shown in Figure 7b shows both the structure of the TiO_2(011)-2 × 1 substrate as well as the new mixed oxide surface. Gridlines indicate the lattice as measured from the TiO_2(011)-2 × 1 substrate structure. This allows determination of the protrusions in the mixed oxide relative to the TiO_2 lattice. Furthermore, linear defects or domain boundaries are frequently observed in STM images of the mixed oxide surface phase. This is shown in Figure 7b,c. These straight domain boundaries are aligned with the ⟨01−1⟩ substrate direction. The unit cells marked in Figure 7c show that these domain boundaries correspond to a ∼1/2 unit cell offset between neighboring domains. In order to determine a possible atomic-scale structural model for this surface structure, we performed DFT simulations that are discussed next.

Computational. Mixed oxide surfaces may exhibit complicated structures, and therefore, computational simulation and screening of possible structural models are still challenging. In particular, a robust optimization strategy other than those based on bulk-truncated substrates with arbitrary construction of add-on dopants is highly desired. In the current work, an evolutionary algorithm was adopted in combination with total energy DFT calculations for generating and optimizing structures. The 2 × 1 rutile TiO_2(011) surface cells containing a full (4 FeO) or half (2 FeO) monolayer of FeO units (with respect to the number of surface TiO_2 units) on top were considered in the search for possible mixed $FeTiO_x$ surface oxides. The calculation details are given below.

For each 2 × 1 surface cell of rutile TiO_2(011), four TiO_2 units are exposed, and they have the same height on an unreconstructed surface while two of them rise above the other two on a 2 × 1 reconstructed surface.[8] We first performed calculations to search for the mixed oxide surface containing a full monolayer of FeO (4 FeO). The calculated structures with the lowest and second lowest total energies are illustrated in Figure 8a,b. One can see that the most stable mixed oxide surface exhibits disordered structure, while the second most stable surface structure is very ordered and quite similar to the ilmenite (012) surface, which is illustrated in Figure 8c. More oxide surfaces with mixed FeO and TiO_2 in the top two surface layers were also calculated (see Figure 8d,e) in order to further test the stability of ilmenite-type mixed surfaces. As one can see from Table 1, the determined well-ordered structures are significantly less stable compared to the disordered one, and the tested multilayer ilmenite-type mixed

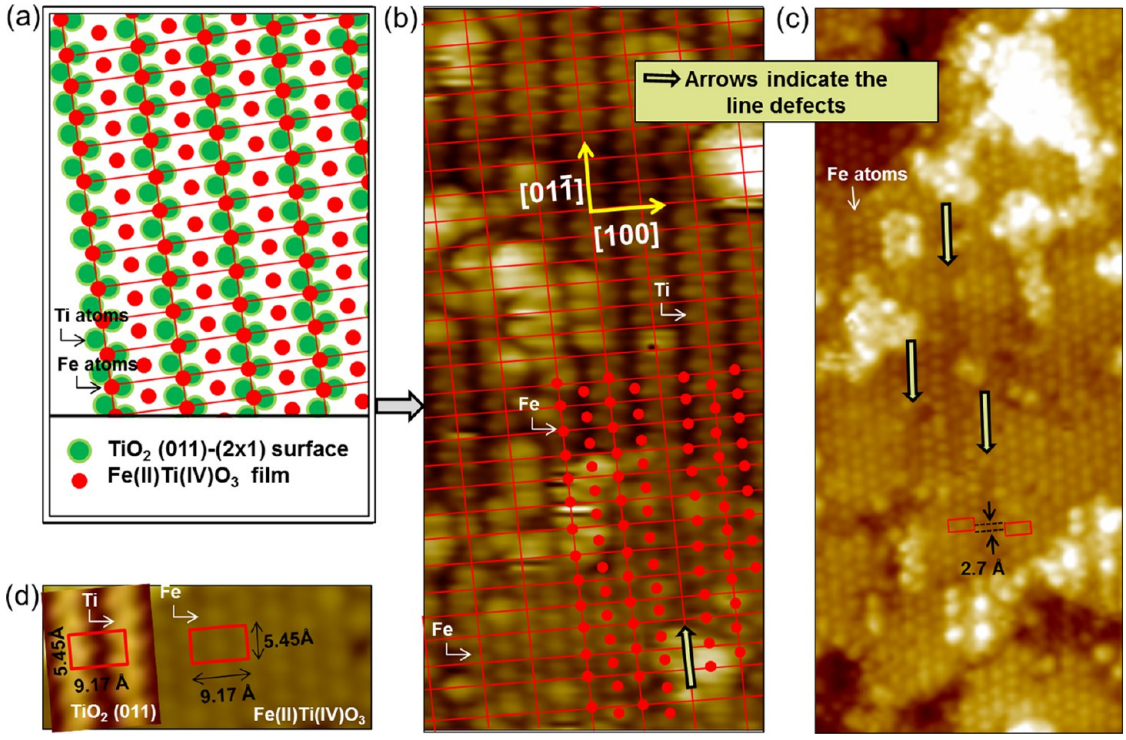

Figure 7. (a) Top view of the structural model of the new surface mixed oxide phase formed on the TiO_2(011)-2 × 1 reconstructed surface. (b) STM image that shows both the structure of the TiO_2(011)-2 × 1 substrate and the new mixed oxide surface. The gridlines indicate the lattice as measured from the TiO_2(011)-2 × 1 structure. (c) Linear defects or domain boundaries aligned with the [01−1] substrate direction observed in STM images of the mixed oxide surface phase. (d) Rectangular unit cell dimensions given by the TiO_2(011) substrate and the new mixed oxide phase.

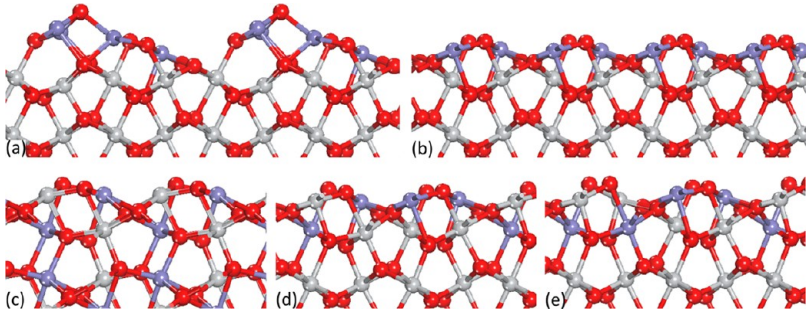

Figure 8. Cross-sectional view of various calculated structural models for a full iron oxide monolayer (a,b,d,e) on a rutile TiO_2(011) surface and that for a bulk ilmenite $FeTiO_3$(012) surface (c). Ti atoms are in gray, O in red, and Fe in violet.

TABLE 1. Calculated Relative Energies of Different Surface Structures with Full and Half Monolayer FeO on Rutile TiO_2(011)

	full monolayer			
structure	Figure 8a	Figure 8b	Figure 8d	Figure 8e
relative energy (ΔE, eV)	0	0.27	0.70	0.93

	half monolayer					
structure	Figure 9a	Figure 9b	Figure 9c	Figure 9d	Figure 9e	Figure 9f
relative energy (ΔE, eV)	0	0.08	0.10	0.11	0.11	0.15

oxides on TiO_2(011) are even less stable. From the above calculated structures and corresponding stability trend of the monolayer FeO at TiO_2(011), one may conclude that Fe cations do not like to form multilayer ordered $FeTiO_3$ structures on TiO_2(011) substrates. Furthermore, when the Fe cations all occur at the surface, repulsion between them prevents the formation of uniformly distributed FeO units.

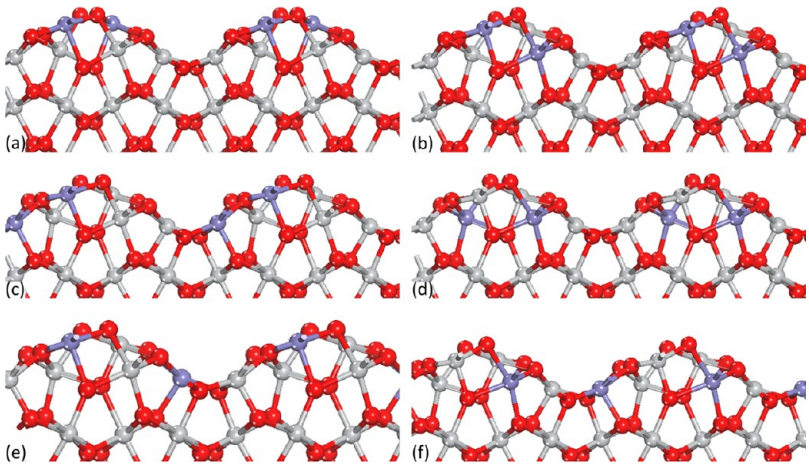

Figure 9. Cross-sectional view of various calculated structural models for half a monolayer of iron oxide on a rutile TiO_2(011) surface. Ti atoms are in gray, O in red, and Fe in violet.

From these results, it can be suggested that a full monolayer of FeO may not match well with the TiO_2-(011) substrate. Consequently, one may expect that a submonolayer of FeO could be more favorable for formation of an ordered mixed oxide surface layer. Therefore, we also calculated the mixed surface oxide with a half monolayer of FeO (*i.e.*, two FeO in each 2 × 1 surface cell). The obtained six structures with the lowest total energies are illustrated in Figure 9a–f in order of stability. In this case, one can see that the most stable mixed surface oxide (Figure 9a) gives an ordered structure that appears to form by removing half of the ordered full monolayer FeO (Figure 8a). It needs to be noted that, though such structures look similar to that of the ilmenite (012), clear differences exist between these structures; particularly, the Ti and Fe cations are not uniformly mixed in the obtained surface structure, but the two FeO units actually form a dimer row anchored at the pristine TiO_2 support. In fact, the ilmenite-like structures with dispersed FeO (Figure 9b–f) were calculated to be much less stable. Furthermore, the mixed surface oxide with the TiO_2(011) substrate in a reconstructed (disordered) configuration was also found to be unstable (not shown).

Thus, from calculated structures and energetics of the mixed oxide surface, the observed ordered $FeTiO_x$ surface can be explained by the half monolayer FeO model shown in Figure 9a. This structure exhibits an equal number of exposed Fe^{2+} and Ti^{4+} cations on the surface, which is consistent with the experimental ISS measurement. We also simulated the STM image of this surface, shown in Figure 10. It can be seen that the exposed Fe^{2+} gives the brightest features. The 2 × 1 unit cell structure of the structural model is also clearly represented in the calculated STM images. In contrast, the experimental STM image appears like a c(2 × 1) structure. This may indicate that tip effects in the strongly corrugated structure play an important role in the imaging of this structure, more sophisticated

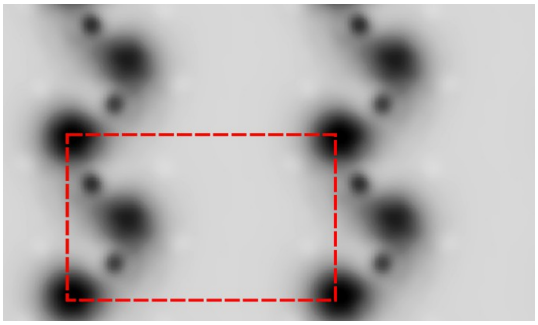

Figure 10. Simulated STM images of the most stable half monolayer FeO structure at rutile TiO_2(011) (Figure 9a). The large bright spots correspond to Fe cations and small spots to topmost O. The dotted square in red indicates the (2 × 1) unit cell.

STM simulations need to be employed,[20] or yet other structures exist. Finally, we want to point out that, although the whole top layer TiO_2 as well as the added FeO were included in the mixed oxide structure search, no reconstruction as that of TiO_2(011)-2 × 1 was determined to favorably occur for the substrate. This suggests that the FeO deposition can remove the reconstruction of the clean TiO_2(011) surface, similar to the case of adsorptions of various organic molecules.[21] Moreover, from the optimized structure, one could also see that both the exposed Ti and Fe cations at the surface exhibit dangling bonds, which can give rise to unique chemical properties of such a mixed oxide surface.

CONCLUSIONS

This work demonstrates that well-ordered surface structures of monolayer mixed oxides may be obtained on single-crystal surfaces under the right preparation conditions, and thus novel mixed oxide monolayer materials can be synthesized and characterized by surface science investigations. While there are many more investigations of monolayer oxides on the rutile TiO_2(110) surface, very few similarly well-ordered oxide

monolayers[22,23] have been reported for that surface orientation. We consider that the less stable (011) surface that exhibits a 2 × 1 surface reconstruction may facilitate the formation of ordered mixed oxide surfaces. In the particular case of iron oxide on TiO_2, the formed mixed oxide surface layer has similarities with the ilmenite $FeTiO_3$ phase from both a structural perspective as well as the cation charge states. Iron is not the only transition metal that forms the ilmenite structure with TiO_2. Other metals that form a mixed oxide ilmenite phase with Ti include Mn, Ni, Co, Mg, and also V. Thus, it will be exciting to investigate if the same bulk structure of these mixed oxides can also be translated in the formation of the same surface mixed oxide on TiO_2(011). Identification, synthesis, and compositional control of well-ordered mixed oxide monolayers are prerequisites for atomic-scale understanding of these kinds of nanocatalysts. The studies reported here suggest that the TiO_2(011) surface is a better model system for these kinds of investigations than the more frequently used rutile TiO_2(110) surface.

METHODS

Experimental Methods. STM studies were performed in an UHV chamber with a base pressure of $\sim 2 \times 10^{-10}$ Torr equipped with an Omicron variable temperature (VT)-STM operated at room temperature. Empty-state STM images were recorded at room temperature with electrochemically etched tungsten tips cleaned *in situ* by voltage pulsing. XPS, UPS, and ISS measurements were performed in a separate UHV chamber with a base pressure of $\sim 5 \times 10^{-10}$ Torr. This second UHV chamber was also equipped with a room temperature STM, which was used to make sure that the same surface structures were obtained. For electron and ion spectroscopy studies, a non-monochromatized dual-anode X-ray source (Omicron, DAR 400) for XPS, a He II VUV photon source (Omicron, HIS 13) for UPS, and a fine focused ion (He^+ ions with primary energy of ~1000 eV) gun for ISS measurements were used. The kinetic energy of the scattered electrons/ions were detected with a seven-channel hemispherical energy analyzer (Omicron, Sphera II). To increase the surface sensitivity in XPS measurements, data were collected with the analyzer at a grazing angle of 70° (measured from surface normal). For UPS and ISS, the analyzer was normal to the surface. The scattering angle for ISS was 37° in our experimental setup. The XPS data were acquired with Mg Kα X-rays. The XPS peaks were fitted with Gaussian−Lorentzian peak shape after subtracting a Shirley background. Substrate preparation and the methodology for iron deposition as well as the subsequent annealing procedures were identical in the two UHV systems. Briefly, the commercially available TiO_2(011) single-crystal substrate (from MTI Corporation) was prepared by multiple cycles of Ar^+ sputtering at room temperature (1 kV, 5 μA, 30 min) followed by UHV annealing at 700 °C for 30 min. The cleanliness of the surface was checked by STM. Fe was evaporated from an Fe rod and heated in a water-cooled mini e-beam evaporator with the substrate held at room temperature. The 2, 4, and 7 min exposure periods were estimated from STM images to correspond to 0.25, 0.5, and 0.75 ML surface coverage, respectively.

Computational Methods. In this work, we used the evolutionary algorithm embedded in USPEX code[24−29] to search for stable surface structures, which has been successfully applied for predicting stable structures of bulk crystals,[25] nanoclusters,[26] surfaces,[27] and polymers.[29] As a global optimization method, the USPEX code uses four ways (hereditary, mutation, transmutation, random) to produce surface structures, and the whole prediction usually requires hundreds or thousands of individual structure relaxations. In our calculations, oxide surfaces were modeled by periodic slabs; each candidate surface structure can be divided into vacuum, surface, buffer, and substrate regions, and only the surface region was involved in generating new structures.[27] In the current work, calculated lattice parameters of bulk rutile TiO_2 are $a = b = 4.660$ Å, $c = 2.973$ Å, in good agreement with experimental values. The unreconstructed and 2 × 1 reconstructed rutile TiO_2(011) surfaces were modeled with a slab containing four TiO_2 layers in a 2 × 1 surface cell. The vacuum height was about 15 Å. In the structural optimization, we relaxed the atom positions in the surface and buffer region, while the other atoms (bottom two layers of the TiO_2(011)) were fixed. In our calculations, the relaxations were done using DFT calculations within the generalized gradient approximation (GGA)[30] using the all-electron projector-augmented wave[31] method as implemented in the VASP code.[31,32] We used the kinetic energy cutoff of 400 eV for the plane wave basis set. The Brillouin zone was sampled with a 1 × 2 × 1 *k*-point mesh, and each candidate structure was relaxed until the residual forces were below 0.05 eV/Å.

In order to reduce the computing time, we took the topmost O of the unreconstructed rutile TiO_2(011) layer together with all the added FeO (4 in a unit cell) as the surface layer for calculating the mixed surface oxide with a full monolayer FeO. In contrast, for calculating the mixed surface oxide with half monolayer FeO, we then took the whole top TiO_2 layer together with the added FeO (2 in a unit cell) as the surface layer. Details of the STM simulations[33] can be found in our early work.[8,21]

Conflict of Interest: The authors declare no competing financial interest.

Acknowledgment. The USF group acknowledges support from the U.S. Department of Energy-Office of Basic Energy Sciences under DE-FG02-09ER1608 and the National Science Foundation under CHE-1505609. The ECUST group acknowledges the financial support from the National Basic Research Program (2011CB808505), National Natural Science Foundation of China (21421004, 21322307), "Shu Guang" project of Shanghai Municipal Education Commission and Shanghai Education Development Foundation (13SG30), and the Fundamental Research Funds for the Central Universities (WD1313009). National Super Computing Center in Jinan is also acknowledged for computing time.

REFERENCES AND NOTES

1. Artiglia, L.; Agnoli, S.; Savio, L.; Pal, J.; Celasco, E.; Rocca, M.; Bondino, F.; Magnano, E.; Castellarin-Cudia, C.; Netzer, F. P.; et al. From Vanadia Nanoclusters to Ultrathin Films on TiO_2(110): Evolution of the Yield and Selectivity in the Ethanol Oxidation Reaction. *ACS Catal.* **2014**, *4*, 3715–3723.
2. Colussi, S.; Gayen, A.; Camellone, M. F.; Boaro, M.; Llorca, J.; Fabris, S.; Trovarelli, A. Nanofaceted Pd-O Sites in Pd-Ce Surface Superstructures: Enhanced Activity in Catalytic Combustion of Methane. *Angew. Chem., Int. Ed.* **2009**, *48*, 8481.
3. Mullins, D. R. The Surface Chemistry of Cerium Oxide. *Surf. Sci. Rep.* **2015**, *70*, 42–85.
4. Diebold, U. The Surface science of Titanium Dioxide. *Surf. Sci. Rep.* **2003**, *48*, 53–229.
5. Henderson, M. A. A Surface Science Perspective on TiO_2 Photocatalysis. *Surf. Sci. Rep.* **2011**, *66*, 185–297.
6. Beck, T. J.; Klust, A.; Batzill, M.; Diebold, U.; Di Valentin, C.; Selloni, A. Surface Structure of TiO_2(011)-(2 × 1). *Phys. Rev. Lett.* **2004**, *93*, 036104.

7. Torrelles, X.; Cabailh, G.; Lindsay, R.; Bikondoa, O.; Roy, J.; Zegenhagen, J.; Teobaldi, G.; Hofer, W. A.; Thornton, G. Geometric Structure of TiO_2(011)(2 × 1). *Phys. Rev. Lett.* **2008**, *101*, 185501.
8. Gong, X. Q.; Khorshidi, N.; Stierle, A.; Vonk, V.; Ellinger, C.; Dosch, H.; Cheng, H. Z.; Selloni, A.; He, Y. B.; Dulub, O.; et al. The 2 × 1 Reconstruction of the Rutile TiO_2(011) Surface: A Combined Density Functional Theory, X-ray Diffraction, and Scanning Tunneling Microscopy Study. *Surf. Sci.* **2009**, *603*, 138–144.
9. Setvin, M.; Daniel, B.; Mansfeldova, V.; Kavan, L.; Scheiber, P.; Fidler, M.; Schmid, M.; Diebold, U. Surface Preparation of TiO_2 Anatase (101): Pitfalls and How to Avoid Them. *Surf. Sci.* **2014**, *626*, 61–67.
10. Busiakiewicz, A. Temperature-Dependent Composition of Fe/TiO_2(110) and Fe/TiO_2(001) Interfaces. *Appl. Surf. Sci.* **2014**, *311*, 391–398.
11. Diebold, U.; Pan, J. M.; Madey, T. E. Ultrathin Metal Film growth on TiO_2(110): an Overview. *Surf. Sci.* **1995**, *331−333*, 845–854.
12. Pan, J. M.; Maschhoff, B. L.; Diebold, U.; Madey, T. E. Structural Study of Ultrathin Metal Films on TiO_2 using LEED, ARXPS and MEED. *Surf. Sci.* **1993**, *291*, 381–394.
13. Tao, J. G.; Batzill, M. Role of Surface Structure on the Charge Trapping in TiO_2 Photocatalysts. *J. Phys. Chem. Lett.* **2010**, *1*, 3200–3206.
14. Batzill, M.; Morales, E. H.; Diebold, U. Surface Studies of Nitrogen Implanted TiO_2. *Chem. Phys.* **2007**, *339*, 36–43.
15. Yim, C. M.; Pang, C. L.; Thornton, G. Oxygen Vacancy Origin of the Surface Band-Gap State of TiO_2(110). *Phys. Rev. Lett.* **2010**, *104*, 036806.
16. Raghavender, A. T.; Hoa Hong, N.; Joon Lee, K.; Jung, M. H.; Skoko, Z.; Vasilevskiy, M.; Cerqueira, M. F.; Samantilleke, A. P. Nano-Ilmenite $FeTiO_3$: Synthesis and Characterization. *J. Magn. Magn. Mater.* **2013**, *331*, 129–132.
17. Tang, X.; Hu, K. A. The Formation of Ilmenite $FeTiO_3$ Powders by a Novel Liquid Mix and H_2/H_2O Reduction Process. *J. Mater. Sci.* **2006**, *41*, 8025–8028.
18. Ginley, D. S.; Butler, M. A. The Photoelectrolysis of Water Using Iron Titanate Anodes. *J. Appl. Phys.* **1977**, *48*, 2019–2021.
19. Tao, J. G.; Luttrell, T.; Batzill, M. A Two-dDmensional Phase of TiO_2 with a Reduced Bandgap. *Nat. Chem.* **2011**, *3*, 296–300.
20. Woolcot, T.; Teobaldi, G.; Pang, C. L.; Beglitis, N. S.; Fisher, A. J.; Hofer, W. A.; Thornton, G. Scanning Tunneling Microscopy Contrast Mechanisms for TiO_2. *Phys. Rev. Lett.* **2012**, *109*, 156105.
21. Cuan, Q. C.; Tao, J. G.; Gong, X. Q.; Batzill, M. Adsorbate Induced Restructuring of TiO_2(011)-(2 × 1) Leads to One-Dimensional Nanocluster Formation. *Phys. Rev. Lett.* **2012**, *108*, 106105.
22. Zhang, L. O.; Li, M.; Diebold, U. Characterization of Ca Impurity Segregation on the TiO_2(110) Surface. *Surf. Sci.* **1998**, *412−413*, 242–251.
23. Bikondoa, O.; Pang, C. L.; Muryn, C. A.; Daniels, B. G.; Ferrero, S.; Michelangeli, E.; Thornton, G. Ordered Overlayers of Ca on TiO_2(110)-1 × 1. *J. Phys. Chem. B* **2004**, *108*, 16768–16771.
24. Martoňák, R.; Oganov, A. R.; Glass, C. W. Crystal Structure Prediction and Simulations of Structural Transformations: Metadynamics and Evolutionary Algorithms. *Phase Transitions* **2007**, *80*, 277–298.
25. Lyakhov, A. O.; Oganov, A. R.; Valle, M. How to Predict Very Large and Complex Crystal Structures. *Comput. Phys. Commun.* **2010**, *181*, 1623–1632.
26. Lyakhov, A. O.; Oganov, A. R.; Stokes, H. T.; Zhu, Q. New developments in Evolutionary Structure Prediction Algorithm USPEX. *Comput. Phys. Commun.* **2013**, *184*, 1172–1182.
27. Zhu, Q.; Li, L.; Oganov, A. R.; Allen, P. B. Evolutionary Method for Predicting Surface Reconstructions with Variable Stoichiometry. *Phys. Rev. B: Condens. Matter Mater. Phys.* **2013**, *87*, 195317.
28. Valle, M.; Oganov, A. R. Crystal Fingerprint Space- a Novel Paradigm for Studying Crystal-Structure Sets. *Acta Crystallogr., Sect. A: Found. Crystallogr.* **2010**, *66*, 507–17.
29. Sharma, V.; Wang, C. C.; Lorenzini, R. G.; Ma, R.; Zhu, Q.; Sinkovits, D. W.; Pilania, G.; Oganov, A. R.; Kumar, S.; Sotzing, G. A.; et al. Rational Design of all Organic Polymer Dielectrics. *Nat. Commun.* **2014**, *5*, 4845.
30. Perdew, J. P.; Burke, K.; Ernzerhof, M. Generalized Gradient Approximation Made Simple. *Phys. Rev. Lett.* **1996**, *77* (18), 3865.
31. Kresse, G.; Furthmüller, J. Efficient Iterative Schemes for *Ab Initio* Total-Energy Calculations Using a Plane-Wave Basis Set. *Phys. Rev. B: Condens. Matter Mater. Phys.* **1996**, *54*, 11169.
32. Kresse, G.; Hafner, J. *Ab initio* Molecular Dynamics for Liquid Metals. *Phys. Rev. B: Condens. Matter Mater. Phys.* **1993**, *47* (1), 558.
33. Tersoff, J.; Hamann, D. R. Theory and Application for the Scanning Tunneling Microscope. *Phys. Rev. Lett.* **1983**, *50*, 1998–2001.